Toughness and Microstructure of 13Cr4NiMo High-Strength Steel Welds

P. Bilmes, C. Llorente, and J. Pérez Ipiña

(Submitted 4 April 2000; in revised form 22 August 2000)

The microstructures and tensile, Charpy, and crack tip opening displacement (CTOD) properties of 13Cr4NiMo soft martensitic stainless steel flux cored arc welding process (FCAW) weld metals have been studied through different applied postweld heat treatments (PWHT). Phases and microstructural characteristics have been analyzed by scanning electron microscopy (SEM) and x-ray diffraction. The effect of the tempering and double tempering, with and without previous solution annealing, on the impact and fracture toughness has been studied. The role of the retained austenite resulting from tempering has been recognized, and it is suggested that the austenite particles improve the toughness of the welds through their transformation by the transformation-induced plasticity (TRIP) mechanism.

Keywords mechanical properties, microstructure, postweld heat treatment, retained austenite, soft martensitic stainless steel

1. Introduction

The poor weldability of martensitic stainless steels, their sensivity to cold cracking, and the unsatisfactory mechanical properties in the welded joints led to the development of low-carbon (soft) martensitic stainless steels in the 1960s.[1]

If the 12% Cr stainless steels are used as high-strength steels, they have to be weldable, formable, and have good toughness.[2] Hence, in soft martensitic stainless steels, the carbon content is kept below mass 0.1% to improve weldability by promoting a structure with less tendency to cold cracking, better corrosion resistance, and better toughness. In addition, they have high strength with high toughness and ductility even at very low temperatures or thick cross sections.[3,4] Due to low carbon, the addition of 4 to 6% Ni (the most powerful austenite former after C and N) is required to avoid a significant content of δ-ferrite, which is deleterious to both impact and fracture toughness. For enhanced corrosion resistance together with resistance to temper embrittlement and tempering, 0.5 to 2% molybdenum is added, depending on the intented use.

The characteristics of such 13Cr-4NiMo soft martensitic stainless steels have resulted in an increasingly worldwide use and this trend is expected to continue.[5] The uses of such steels are in petrochemical and chemical plants or industries, gas turbine engines, turbine blades, hydraulic turbines, valve bodies, pump bowls, compressor cones and discs, and in a variety of aircraft structural and engine applications.[5,6,7]

The weld metals of 13Cr-4NiMo steels have martensitic microestructures in the as-welded condition; therefore, they normally require postweld heat treatments (PWHT) to satisfy the service requirements.[8] If high toughness values are required, even in subzero temperatures, PWHT such as intercritical tempering or solution annealing plus intercritical tempering or double (high plus intercritical) tempering can be necessary.[9] The solution annealing is performed at temperatures between 950 and 1050 °C. The aim of such treatment is the homogenization of the structure by dissolution of the δ-ferrite and retained austenite, which are nonequilibrium solidification products. The intercritical tempering at 600 °C produces a softening of martensite and a finely dispersed austenite that is stable and nontransformable during cooling. It is known that such austenite, which can be observed only by scanning electron microscopy (SEM), increases the toughness, although it slightly reduces the strength.

Regarding the relative use of different welding consumable types for welding structural steel, the consumption of tubular wire in the world has markedly increased for the last few years and it is expected to continue increasing rapidly.[5,10] Taking this into account, the purpose of the present work is to study the microstructures resulting from different PWHT applied to 13Cr4NiMo weld metals obtained by means of the flux cored arc welding process (FCAW), together with the effects on their tensile, Charpy V-notch impact, and crack tip opening displacement (CTOD) properties. In addition, the role of the most important phases in the microstructures is considered and correlated with the mechanical properties.

2. Experimental

The FCAW process was used to prepare the weld metals. Multiple-pass welds were performed on AISI 410 plates using an E410NiMoT-2 welding wire, according to AWS A.5.22. The composition of the welding wire and the welding parameters are shown in Tables 1 and 2. The multiple-pass weld performed by FCAW was cut in five parts to apply different PWHT so that five test coupons (one condition as-welded and four with different PWHT) were obtained for testing.

P. Bilmes, Department of Mechanics, School of Engineering, National University of La Plata and CONICET, La Plata, Argentina; **C. Llorente**, Department of Mechanics, School of Engineering, National University of La Plata and CICPBA, La Plata, Argentina; and **J. Pérez Ipiña**, School of Engineering, National University of Comahue and CONICET, Neuquén, Argentina. Contact e-mail: pabilmes@volta.ing.unlp.edu.ar.

The PWHT were intercritical temperings at 600 °C/2 h and double temperings (670 °C/2 h + 600 °C/2 h), with and without previous solution annealing at 950 °C/1 h (Table 3). The chemical composition of the weld metals in different conditions was measured by an optical emission technique (except for C, N, O, and S, which were measured by combustion analysis). A scanning electron microscope operated at 25 kV was used to analyze the microstructures of the weld metals and the fracture surfaces of the specimens for impact and fracture toughness testing. Samples were ground and electropolished. The electrolyte composition for electropolishing was $HClO_4$: 62 mL, ethanol: 700 mL, butyl cellusolve: 100 mL, and H_2O: 137 mL. Then, specimens were etched in Vilella's solution.

To identify austenite and to measure its volume fraction in each weld condition, x-ray diffraction applying a Rietveld analysis was used. The x-ray diffraction patterns were obtained at room temperature with a diffractometer furnished with a diffracted beam graphite monochromator. Data were collected using Cu K_α radiation in the range of $10 \leq 2\theta \leq 120$ at a step interval of 0.02°. A Rietveld analysis was performed using the program DBWS-9411.[11] The sample displacement and the background (modeled with a fifth degree polynomial) were refined independently but not simultaneously, as well as the unit cell, the preferred orientation, the Pseudo-Voigt profile parameters, and the scale factor of different phases present in the sample. From the Rietveld analysis, a relative weight fraction was assigned to the refined phases. This approximation disregards the contributions of all other minor phases. The accuracy, in the phase abundance results, was calculated from the scale factors and from estimated volume standard deviations.

Mechanical properties were evaluated by means of tensile, Charpy V-notch impact, Rocwell-C hardness, and microhardness tests according to ASTM A 370. The Charpy V-notch impact tests were carried out at 20 and −77 °C. Microhardness was measured by using a Vickers meter with a load of 20 g and a loading time of 15 s. Fracture toughness was evaluated by means of CTOD tests through critical CTOD or maximum load CTOD at room temperature on compact specimens 0.5 in. thick (1/2 ″ T-CT) according to ASTM E-1290.

Table 1 Nominal composition of the consumable (wt.%)

Consumable (AWS A5.22)	Wire ∅ (mm)	C	Si	Mn	Cr	Ni	Mo
E410NiMoT-2	2.4	0.06	1	1	11–12.5	4–5	0.4–0.7

Table 2 Welding parameters

Gas	Gas flow (LPM)	Voltage (V)	Current DC+ (A)	Arc speed (cm/min)	Interpass temperature (°C)
Ar/2%O_2	20	26–28	300–315	15–16	<130

3. Results and Discussion

The results of the chemical composition of the weld metals in the as-welded condition and with different applied PWHT are given in Table 4 and show similar compositions for all weld conditions.

The microstructural analysis, tensile properties, hardness, Charpy, and CTOD values obtained for all weld conditions are summarized in Table 5.

In the as-welded condition (A), the microstructure is basicly martensite with some delta ferrite and some retained austenite resulting from nonequilibrium solidification (Fig. 1). Intercritical temperings at 600 °C produce the softening of martensitic structures and a fine dispersion of precipitated austenite does not transform during cooling.

In the intercritical tempering conditions (B and C), the austenite contents evaluated by means of Rietveld analysis are similar. Values are also similar in the double tempering conditions (D and E) (670 °C/2 h + 600 °C/2 h), but they are about 40% higher than the B and C conditions. The microstructure of condition E is shown in Fig. 2.

Delta ferrite has been solution annealed and the structure has been more uniformly regenerated in conditions C and E, which have had solution annealing prior to tempering. The microstructures of conditions C and E both consisted of a mixture of tempered martensite and precipitated austenite.

The fracture modes of Charpy specimens were ductile in all PWHT conditions. Typical dimpled-rupture fracture surfaces have been observed by SEM (Fig. 3). Austenite particles have been observed inside the tiny dimples, although some nonmetallic inclusions were also present in larger dimples. It would seem that after an extensive deformation, microvoids coalesced

Table 3 Applied postweld heat treatments

Test coupons	PWHT	Temperature (°C)	Time (h)	Cooling
A	As-welded PWHT is not applied	…	…	…
B	Intercritical tempering	600	2	Air
C	Solution annealing	950	1	Air
	+			
	Intercritical tempering	600	2	Air
D	Double tempering (High + intercritical)	670 + 600	2 + 2	Air/Air
E	Solution annealing	950	1	Air
	+			
	Double tempering (High + intercritical)	670 + 600	2 + 2	Air/Air

from austenite/matrix interfaces, as has been observed close to the fracture of Charpy specimens (Fig. 4).

The fracture mode of CTOD specimens was also ductile in all PWHT conditions except for condition B, which was brittle. The fracture mode was also brittle in the as-welded condition A. Typical dimpled-rupture fracture surfaces have been observed by SEM in all weld conditions (Fig. 5), though isolated quasi-cleavage has been observed in conditions A and B. The quasi-cleavage seems to be associated with the presence of large nonmetallic inclusions (Fig. 6(a) and (b)), since a larger particle diameter makes the nucleation of a cleavage crack easier.

Tensile and yield strength, Charpy-V notch impact energy, and CTOD values of welds with different applied PWHT are summarized in Fig. 7. On one hand, from this figure, it can be seen that welds have had moderate differences regarding tensile and yield strength. On the other hand, Charpy and CTOD values have had important differences. The CTOD values have had the same trend of the Charpy values (Fig. 8 and 9).

From Fig. 8 and 9, it can be noted that conditions C and E, which have more uniform microstructures without delta ferrite (both due to the solution annealing), have the highest toughness. Between both conditions, Charpy and CTOD values are higher in the double tempering condition E that had a higher austenite content with a more uniform distribution (Fig. 8). Nevertheless, tensile and yield values are higher in condition C (Fig. 9).

Table 4 Chemical composition of the test coupons (wt.%)

Test coupons	C	Si	Mn	Cr	Ni	Mo	P	S	O	N
A	0.07	0.37	0.64	11.08	3.78	0.53	0.017	0.007	0.038	0.029
B	0.07	0.40	0.64	11.12	3.80	0.53	0.017	0.007	0.037	0.030
C	0.07	0.35	0.63	11.10	3.80	0.52	0.017	0.007	0.038	0.028
D	0.07	0.38	0.62	11.14	3.79	0.53	0.017	0.007	0.039	0.030
E	0.07	0.37	0.62	11.08	3.79	0.53	0.017	0.007	0.038	0.029

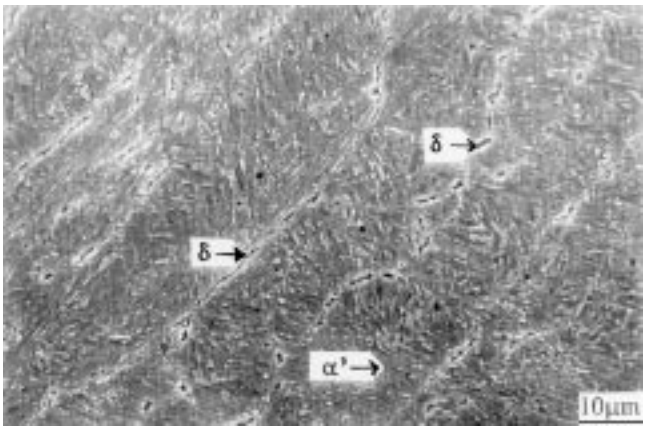

Fig. 1 SEM micrograph of the as-welded weld metal (condition A)

Table 5 Microstructural analysis and mechanical property values obtained for weld conditions A through E

A	B	C	D	E
Delta ferrite(a) Martensite	Delta ferrite(a)		Delta ferrite(a)	
	Tempered martensite	Tempered martensite	Tempered martensite	Tempered martensite
Austenite content(b): (7.6 ± 0.5)	Austenite content(b) (16.1 ± 0.5)	Austenite content(b) (16.2 ± 0.5)	Austenite content(b) (21.8 ± 0.5)	Austenite content(b) (21.2 ± 0.5)
HRC = 37	HRC = 29	HRC = 28	HRC = 25	HRC = 25
Grain size(c) 25 μm	Grain size(c) 25 μm	Grain size(c) 30 μm	Grain size(c) 25 μm	Grain size(c) 30 μm
CTOD (mm) δ_m = 0.037 (δ_c = 0.076)	CTOD (mm) δ_m = 0.122 (δ_c = 0.179) (δ_c = 0.064)	CTOD (mm) δ_m = 0.155 δ_m = 0.160	CTOD (mm) δ_m = 0.152	CTOD (mm) δ_m = 0.166 δ_m = 0.177
YS = 1136 MPa TS = 1189 MPa YS/TS ratio = 0.95	YS = 814 MPa TS = 899 MPa YS/TS ratio = 0.90	YS = 809 MPa TS = 881 MPa YS/TS ratio = 0.92	YS = 784 MPa TS = 871 MPa YS/TS ratio = 0.90	YS = 722 MPa TS = 812 MPa YS/TS ratio = 0.89
δ(%)(d) = 10.8 ψ(%)(e) = 32.8	δ(%)(d) = 17.5 ψ(%)(e) = 59.6	δ((%)(d) = 18.3 ψ(%)(e) = 62.9	δ(%)(d) = 17.5 ψ(%)(e) = 59.6	δ(%)(d) = 23.6 ψ(%)(e) = 64.5
Impact energy CVN at 20 °C: 30 J-100 ps(f) CVN at −77 °C: 18 J/30 ps(f)	Impact energy CVN at 20 °C: 56 J-100 ps(f) CVN at −77 °C: 41 J/95 ps(f)	Impact energy CVN at 20 °C: 83 J-100 ps(f) CVN at −77 °C: 59 J/100 ps(f)	Impact energy CVN at 20 °C: 73 J-100 ps(f) CVN at −77 °C: 47 J/95 ps(f)	Impact energy CVN at 20 °C: 84 J-100 ps(f) CVN at −77 °C: 64 J/100 ps(f)

(a) ≥Vol.5% according to Schaeffler diagram
(b) Vol.% according to Rietveld analysis by x-ray diffraction
(c) Evaluated by means ASTM E 112
(d) Elongation (4∅)
(e) Reduction of area
(f) Percent shear (according to ASTM A 370)

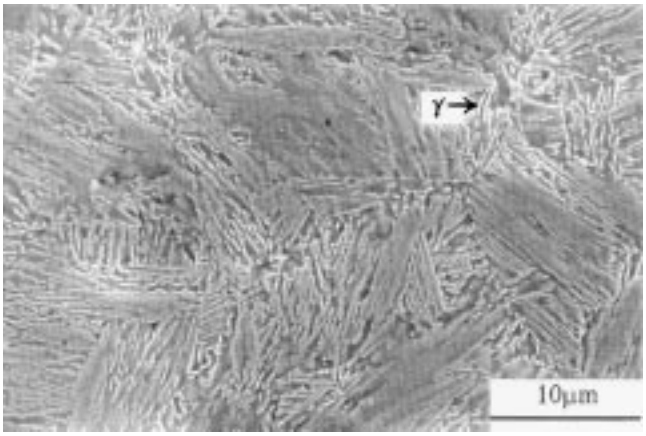

Fig. 2 SEM micrograph of the weld metal with solution annealing plus double tempering (condition E). A fine dispersion of austenite particles can be seen

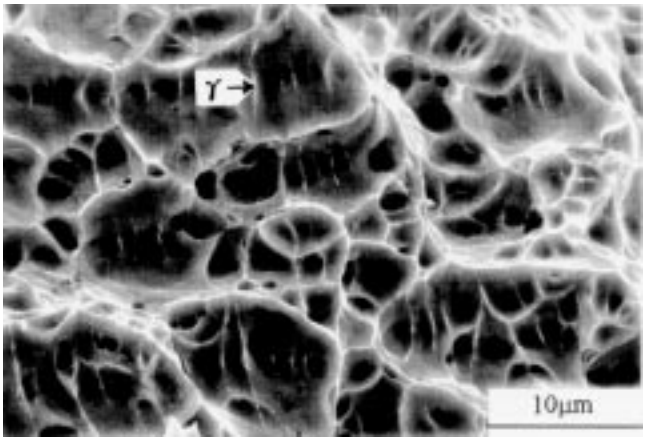

Fig. 3 Typical dimpled-rupture fracture surface observed by SEM in Charpy specimens

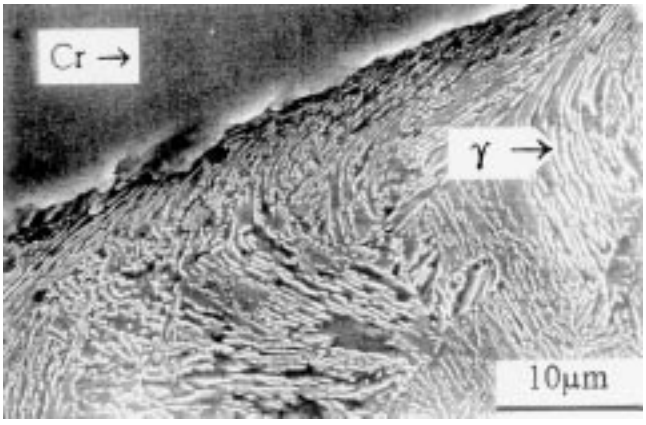

Fig. 4 Microstructure observed by SEM close to the fracture of Charpy specimens. The fracture surface was electroplated with chromium so that metallographic examination could be performed exactly close to the fracture. Microvoids coalesced from austenite/matrix interfaces

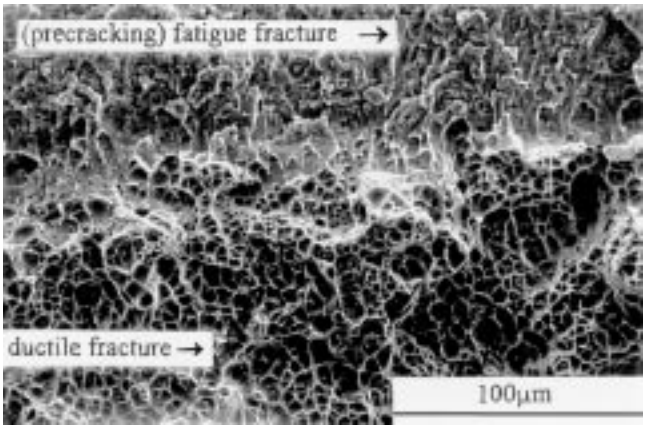

Fig. 5 Typical dimpled-rupture fracture surface observed by SEM in CTOD specimens

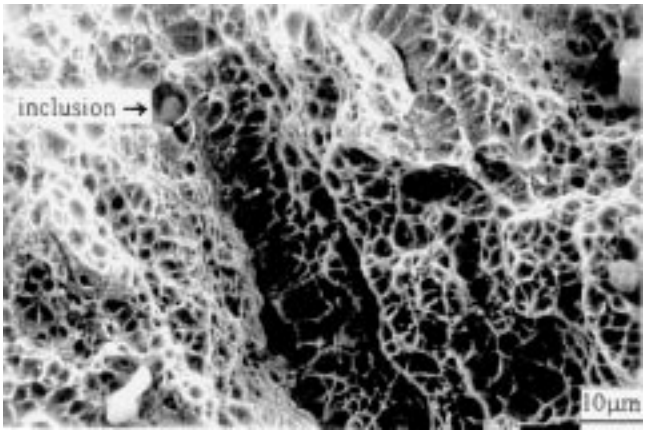

(a)

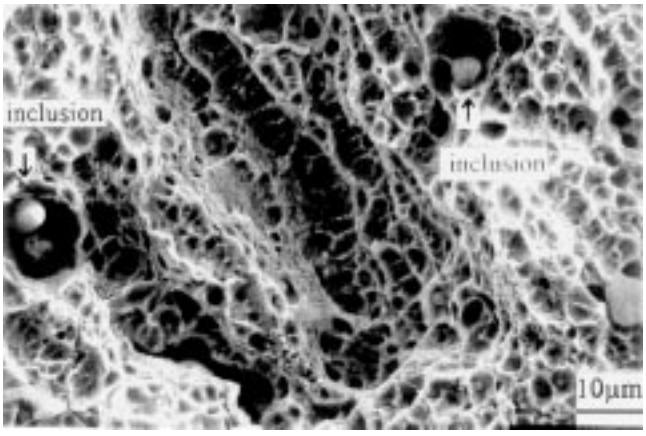

(b)

Fig. 6 CTOD ductile fracture surface with quasi-cleavage associated with the presence of large nonmetallic inclusions: (**a**) condition A and (**b**) condition B

Regarding Charpy values at −77 °C, there has been a slight variation from the values at room temperature, with very little or no percentage of cleavage on the fracture surfaces.

To understand the role of the austenite in the improvement of the toughness of this kind of alloy, regions close to the fracture of tensile, Charpy, and CTOD specimens have been

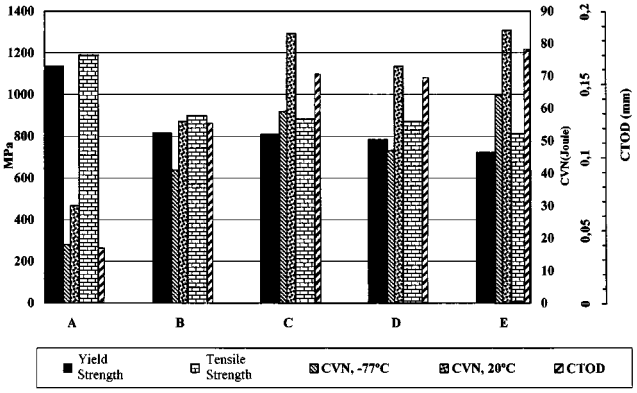

Fig. 7 Tensile and yield strength, Charpy V-notch impact energy, and CTOD values of different welds. A: as-welded condition, and B through E: with different applied PWHT

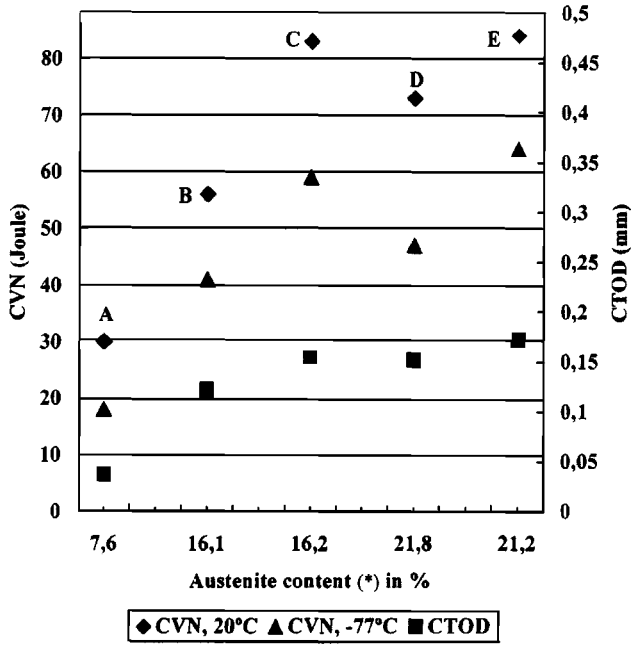

(*) Vol. ± 0.5% according to Rietveld Analysis by x-ray diffraction

Fig. 8 CTOD, Charpy V-notch impact energy, and austenite content values of different welds. A: as-welded condition, and B through E: with different applied PWHT

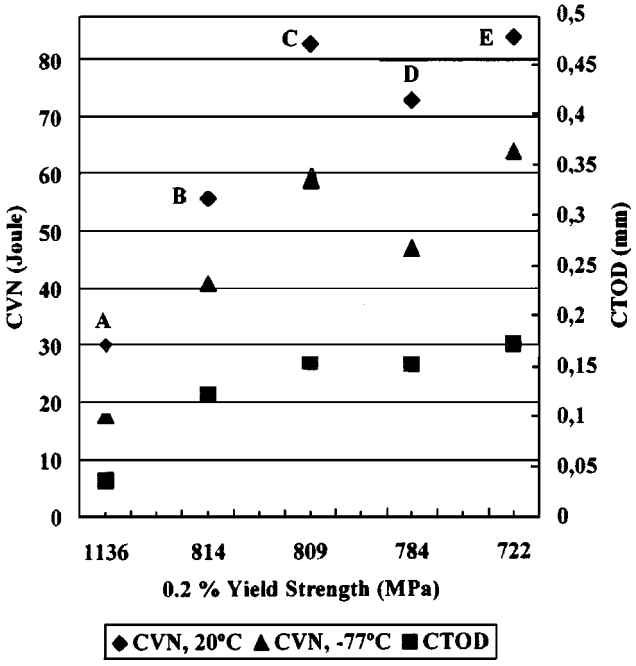

Fig. 9 CTOD, Charpy V-notch impact energy, and yield strength values of different welds. A: as-welded condition, and B through E: with different applied PWHT

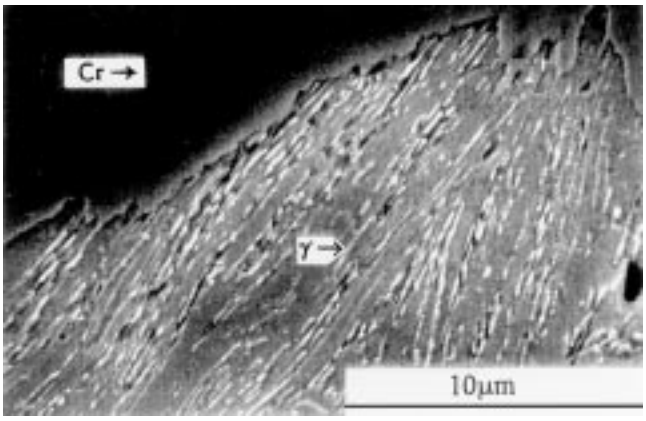

Fig. 10 Microstructure observed by SEM close to the fracture of CTOD specimens. The fracture surface was electroplated with chromium so that metallographic examination could be performed exactly close to the fracture. Microvoids coalesced from austenite/matrix interfaces

analyzed. This study has been carried out on the E condition, corresponding to the applied PWHT that has produced the highest austenite content together with the highest Charpy and CTOD values. The fracture surfaces of the Charpy, CTOD, and tensile specimens were electroplated with chromium so that metallographic examination could be performed exactly close to the fractures (Fig. 4, 10, and 11). From these figures can be noted an important plastic flow, extensive deformation of the austenite particles, and microvoids around both austenite particles and nonmetallic inclusions. These regions have been analyzed by means of microindentation hardness testing. The obtained and averaged Vickers hardness values were 328 HV (33 HRC), which is a higher value than the typical value of this PWHT condition (25 HRC).

To evaluate a mechanical transformation of the austenite particles, x-ray diffraction analysis has been carried out on the regions close to the fracture surfaces of the tensile, Charpy, and CTOD specimens of condition E, where intense deformation fields have been observed. Thus, irregular fracture surfaces were slightly ground and electropolished to prepare smooth surfaces for x-ray diffraction analysis. Figure 12(a) through (d)

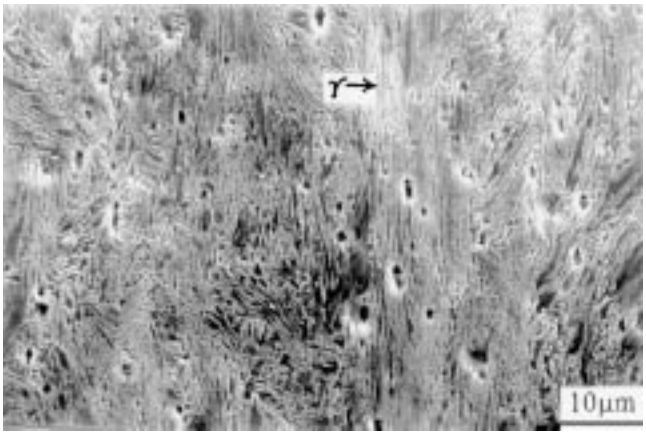

Fig. 11 Microstructure observed by SEM close to the fracture of tensile specimens. Microvoids coalesced from austenite/matrix interfaces and from nonmetallic inclusions

show diffraction patterns of these three regions and the typical diffraction pattern of regions far from the fractures of the three kinds of test specimens. From these figures, it can be seen that austenite is absent in regions close to the fractures and only the ferritic phase is present. Nevertheless, both phases appear far from the fractures.

The absence of austenite in regions immediately close to the fractures together with the hardness increase of these zones plastically deformed may indicate that austenite particles have been transformed into martensite by transformation-induced plasticity (TRIP). It could be suggested that the occurrence of austenite TRIP phenomena in regions with intense deformation fields led to an increased ductility, impact, and fracture toughness of this alloy with finely dispersed austenite. In this last sense, the TRIP mechanism in the plastic zone around a front fracture could absorb energy, effectively contributing to the enhancing of toughness.

4. Conclusions

- Postweld heat treatments have produced the softening of the microstructures together with a finely dispersed austenite precipitation. In the cases of solution annealing previous to temperings and double temperings, more uniform microstructures and without delta ferrite have been obtained. Thus, ductile fractures with typical dimpled-rupture fracture surfaces have been produced. There was correlation between the variation of mechanical properties and the microstructural modifications.
- Higher values of CTOD, Charpy, and ductility have been obtained by means of microstructures composed by tempered martensite and austenite, without delta ferrite. The highest values were obtained from the solution annealing plus double tempering condition, where the austenite content was higher and more uniformly distributed.
- The yield and tensile strength values had slight differences with the applied PWHT. They were lower for the solution annealing plus double tempering PWHT, which produced the maximum softening with the highest ductility and toughness. The decreasing of the yield and tensile strength for all applied PWHT, regarding the as-welded condition, has not been relevant compared to the increase in ductility and toughness.
- The study of the microstructures close to the fractures of

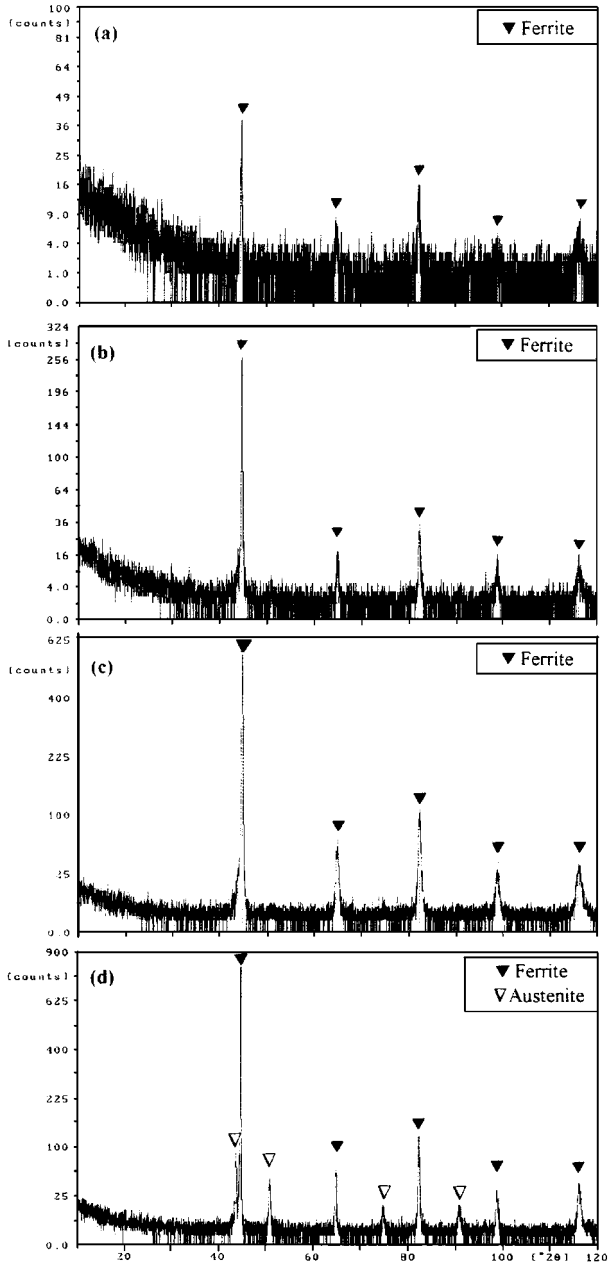

Fig. 12 (**a**) through (**d**) Diffraction patterns of austenite and ferrite: (**a**) close to the fracture of tensile specimens; (**b**) close to the fracture of Charpy speciments; (**c**) close to the fracture of CTOD specimens; and (**d**) typical diffraction pattern of regions far from the fractures of the three kinds of test specimens

tensile, Charpy, and CTOD specimens showed the mechanical transformation of the austenite particles. It is suggested that the beneficial effect of the dispersed austenite on the toughness and ductility of this alloy is based on the localized TRIP mechanism development.

- From Charpy-V notch impact tests, a ductile-brittle transition behavior is not recognized in the range of the tested temperatures. A moderate decrease in the impact energy between −77 °C and room temperature was measured. A higher variation was measured with different applied PWHT at room temperature.

Acknowledgments

The authors acknowledge Consejo Nacional de Investigaciones Científicas y Técnicas (CONICET), Facultad de Ingeniería de la Universidad Nacional de La Plata (UNLP), Comisión de Investigaciones Científicas de la Provincia de Buenos Aires (LEMIT-CICPBA), and Facultad de Ingeniería de la Universidad Nacional del Comahue for financial support. The authors are grateful to Ms. Sci. Mario Sanchez, CICPBA and CINDECA (CONICET-UNLP) Institute, for assistance in the SEM studies and to Eduardo Benotti for preparing and precracking the CTOD specimens.

References

1. E. Folkhard: *Welding Metallurgy of Stainless Steels*, Springer-Verlag, New York, NY, 1988, p. 179.
2. F.B. Pickering: *Physical Metallurgy and the Design of Steels*, Applied Science Publishers, LTD, London, 1978, p. 165.
3. P. Brezina: *Escher Wyss News*, 1980, vol. 53 (1/2), pp. 218-36.
4. H. Niederau: *Stahl Eisen*, 1978, vol. 98 (8), pp. 385-92 (in German).
5. L.E. Svensson and J. Elvander: *Svetsaren*, 1999, vol. 54 (1/2), pp. 3-11.
6. A.W. Marshall and J.C.M. Farrar: Doc:IIW-IX-H-422-98, International Institute of Welding, 1998, p. 3.
7. J.C.M. Farrar and A.W. Marshall: Doc:IIW-IX-H-423-98, International Institute of Welding, 1998, p. 8.
8. T.G. Gooch: *Welding J.*, 1995, vol. 74 (7), pp. 213s-223s.
9. R.D. Kane: *Corros. NACE*, 1977, vol. 33 (7), pp. 231-35.
10. G. Engblom: *Proc. X Congreso Argentino and VI Congreso Iberoamericano de Soldadura*, Welding Society of Argentina, Buenos Aires, 1999, p. 4.
11. R. Young: "Program DBWS-9411 for Rietveld Analysis of X-ray and Neutron Powder Diffraction Patterns," Georgia Institute of Technology, Atlanta, GA, 1994.